# Rhamnopyranoside Pivaloyl Esters as Black and White Fungus Inhibitors: Molecular Docking, Dynamics and ADMET Analysis

Mohammed M. Matin* ⓘ [a], Ajoy Kumer ⓘ [b], Akhel Chandro ⓘ [c], Shopnil Akash ⓘ [d], Unesco Chakma ⓘ [e]

The "Black and White Fungus" is a very infrequently developing pathogen with a high fatality rate that has prompted widespread public health concern during the period of the COVID-19 pandemic. This pathogenic fungus may be widely distributed in nature, in plants, and in deteriorating fruits and vegetables because of its widespread nature. Numerous sugar molecules, such as glucopyranoside and glucofuranose, have been reported to have significant antibacterial, antifungal, and antiviral activity, and they were also revealed to be able to inhibit multidrug-resistant microorganisms. The recent black fungus epidemic was extremely serious in India, combined with COVID-19, which contributed to the high mortality impact and deterioration of the situation due to the unavailability of effective treatments. So, rhamnopyranose type derivatives **1−9** were studied against the proteins associated with black and white fungi such as *Mycolicibacterium smegmatis* (PDB ID 7D6X), *Rhizomucor miehei* (PDB ID 4WTP), *Candida auris* (PDB ID 6U8J), and *Aspergillus luchuensis* (PDB 1BK1). These compounds exhibited favorable physical and biochemical scores, as well as appropriate ADMET metrics, among other characteristics. Following the molecular docking procedure, it was found that **1−9** had the highest binding affinity in most cases, (> -6.00 kcal/mol), while compound **9** had outstanding binding affinity against *Rhizomucor miehei* (-8.7 kcal/mol) and against *Mycolicibacterium smegmatis* (-8.2 kcal/mol). In addition, the binding affinity against white fungus is also outstanding. This time, compounds **8** and **9** had better binding energy, which is -7.8 kcal/mol against *Aspergillus luchuensis* (1BK1) and -7.6 kcal/mol against *Candida auris* (6U8J). Finally, the molecular dynamics simulation at 100 ns has proved that they are stable for new medication development. Among the derivatives **1−9**, ligands **8** and **9** exhibited potential medicinal characteristics when all of the data were considered.

Graphical abstract
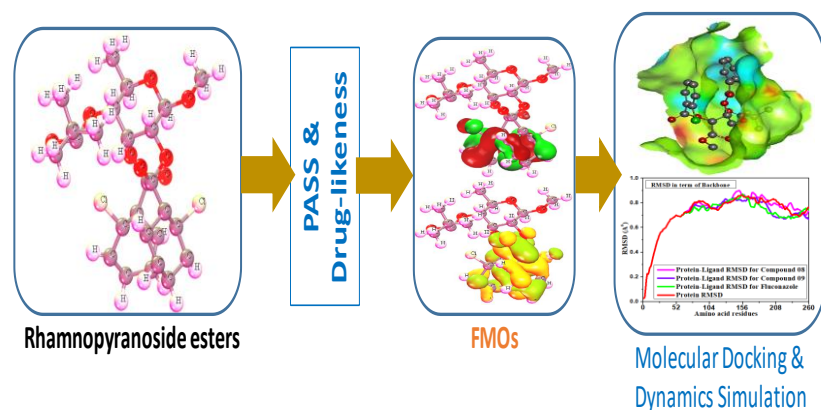
Rhamnopyranoside esters → PASS & Drug-likeness → FMOs → Molecular Docking & Dynamics Simulation

[a] Bioorganic and Medicinal Chemistry Laboratory, Department of Chemistry, University of Chittagong, Chittagong, 4331, Bangladesh. [b] Department of Chemistry, College of Arts and Sciences, IUBAT-International University of Business Agriculture and Technology, 4 Embankment Drive Road, Sector 10, Uttara Model Town, Dhaka, 1230, Bangladesh. [c] Department of Poultry Science, Faculty of Animal Science & Veterinary Medicine, Sher-e-Bangla Agricultural University, Dhaka, 1207, Bangladesh. [d] Department of Pharmacy, Daffodil International University, Sukrabad, Dhaka, 1207, Bangladesh. [e] Department of Electrical and Electronics Engineering, European University of Bangladesh, Gabtoli, Dhaka, 1216, Bangladesh. *Corresponding author. E-mail: **mahbubchem@cu.ac.bd**

1. Introduction

Mucormycosis, often known as "black fungus invasion," is an infrequent but fatal illness that has a risk of death ranging from 46 to 96 percent, according to the ongoing health status of the people [1-3]. During the second phase of the COVID-19 outbreak, or the delta variant phase, the Indian public health service was constantly faced with an existing and new opponent of this deadly black fungal infection [4]. Mucormycosis, or black fungus, is a condition that is characterized by the Mucorales group of fungi and affects different regions of the body [5]. This aggressive fungal disease spreads quickly. Currently, this unusual fungus is infecting COVID-19 sufferers in India at a greater rate than it has ever been before [6, 7]. The occurrence of this black fungus condition is mainly affecting COVID-19 and post-COVID-19 hospitalized sufferers in hospitals, and it is increasing at an alarming rate [7]. As of June 8, 2021, there were 28,252 instances of mucormycosis reported in India. Since the illness has claimed the lives of 4,332 people in India [8]. A total of 86 percent of them had been previously infected by COVID-19, whereas 62.3 percent had a condition such as diabetes [9], while around 65 million people have been affected by diabetes in India [10]. It is anticipated that the exact incidence is far greater than the number of documented cases, according to health professionals. In India, the estimated incidence of black fungus invasion is about 70 times greater than the global data [11]. In typical cases, black fungus impacts the skin as well as interior organs, including the sinuses, brain, lungs, eyes, bones, nerves, and soft tissues [12]. People who suffer from black fungus infections are often plagued by symptoms such as nasal congestion, pain in the eyes and sinuses, and headache [13, 14]. It is difficult to identify this fungal infection earlier since people do not go to clinicians or specialists.

In addition, during the COVID-19 pandemic, the white fungal infection, which is caused by *Candida* and *Aspergillus* species of fungus and spread rapidly [15], also had a significant impact on life. As many as seven recuperating COVID-19 sufferers in the state of Uttar Pradesh, India, have been identified with *aspergillosis*, a serious type of white fungus disease [16]. White fungus disorders are regarded by health authorities as more hazardous than black fungus pathogens [17]. These illnesses are called white fungal due to the white-colored sores that appear on the skin of people who suffer from them. The sores are positioned on the esophagus, create difficulties in digesting food properly, and are frequently detected in the mouth. *Candida auris*, *Aspergillus luchuensis*, and *Candida albicans* are all suspected of being the pathogens responsible for the white disease [18].

Mucormycosis and *Candida auris* are chronic illnesses that require treatment with effective antifungal medication. Currently, amphotericin B has been used to fight against Mucormycosis [19], and it has been documented that amphotericin B is susceptible to *Aspergillus fumigatus* [20]. Besides, azoles are another effective medication for the treatment of black and white fungus. But, in India, research has shown that azoles have also been susceptible to black and white fungal species [21, 22]. On the other hand, among hospitalized patients, *Candida auris* promotes life-threatening infectious diseases that are resistant to multiple drugs [23]. Despite this, no appropriate therapy for white and black fungus has been discovered [24, 25] and is urgently required. Therefore, this research has been investigated to find an effective and potentially useful medication to fight against this deadly fungus infection.

2. Results and Discussion

2.1 Chemistry

Rhamnopyranose is a common carbohydrate-containing compound [26], and the primary goal of this investigation is to identify the antifungal effectiveness of addition or modification of the ester side chain. Therefore, structures **1–9** have been drawn (Figure 1) and optimized for overall computational studies such as molecular docking, molecular dynamics, PASS prediction, etc. These synthetic rhamnopyranoside compounds are already established chemically [27].
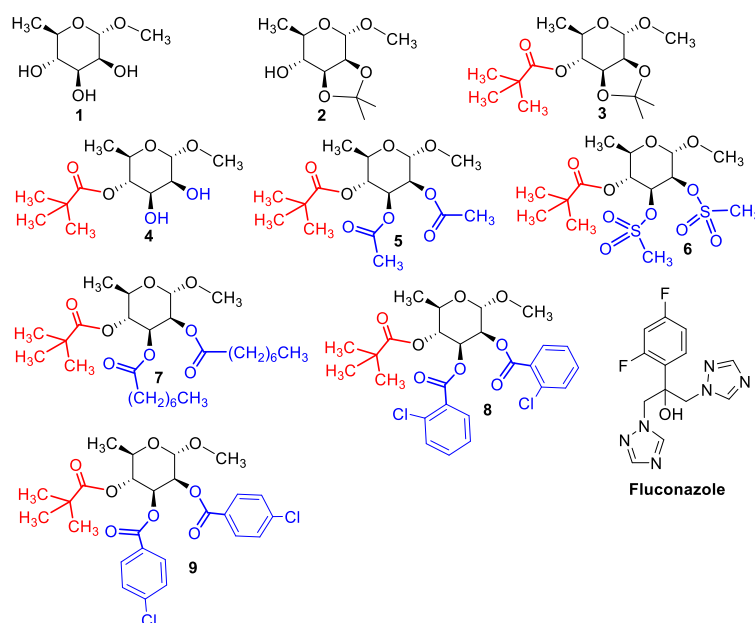

Fig. 1. Chemical structures of rhamnopyranoside **1** and its esters **2-9**.

2.2 Optimized structures

In computational methods, it is crucial to establish the stable complex of each chemical compound before proceeding with further calculations. DFT B3LYP functional and 6-31G++ basis sets have been applied to optimize the geometries of rhamnopyranose **1–9** as represented in Figure 2. The optimized geometries of these molecules revealed that they have a strikingly similar orientation. These optimized, stable arrangements serve as the foundation for all subsequent molecules.
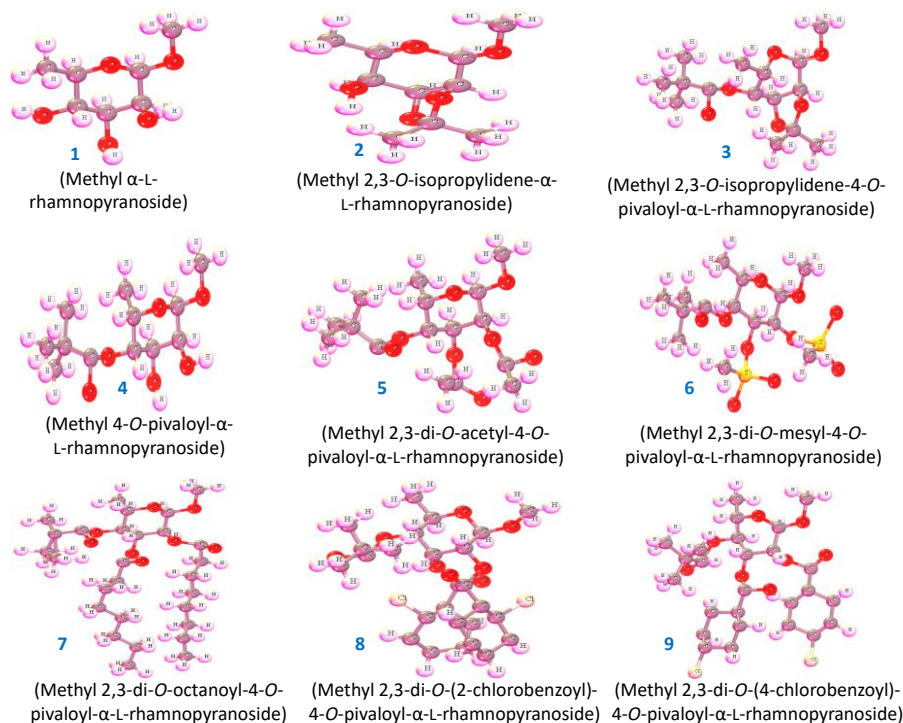

1 (Methyl α-L-rhamnopyranoside)	**2** (Methyl 2,3-*O*-isopropylidene-α-L-rhamnopyranoside)	**3** (Methyl 2,3-*O*-isopropylidene-4-*O*-pivaloyl-α-L-rhamnopyranoside)
4 (Methyl 4-*O*-pivaloyl-α-L-rhamnopyranoside)	**5** (Methyl 2,3-di-*O*-acetyl-4-*O*-pivaloyl-α-L-rhamnopyranoside)	**6** (Methyl 2,3-di-*O*-mesyl-4-*O*-pivaloyl-α-L-rhamnopyranoside)
7 (Methyl 2,3-di-*O*-octanoyl-4-*O*-pivaloyl-α-L-rhamnopyranoside)	**8** (Methyl 2,3-di-*O*-(2-chlorobenzoyl)-4-*O*-pivaloyl-α-L-rhamnopyranoside)	**9** (Methyl 2,3-di-*O*-(4-chlorobenzoyl)-4-*O*-pivaloyl-α-L-rhamnopyranoside)

Fig. 2. Optimized structures of rhamnopyranoside **1** and its esters **2-9**.

2.3 Lipinski rule, pharmacokinetics, and drug-likeness

Drug-likeness in substances must be addressed in the early stages of drug development since it has a significant impact on drug ADMET, GI uptake and disposal, as well as BBB permeability. The Lipinski guidelines (rule of five) state that drug-like compounds must contain the following four characteristics: (i) less than five hydrogen bond donors (HBD); (ii) less than 10 hydrogen bond acceptors (HBA); (iii) more than five NRB; (iv) a molecular mass less than 500 daltons [26]. In Table 1, the HBD, HBA, NRB, MW, log Po/w, log S, Lipinski rules, bioavailability scores, and GI absorption are listed. It has been seen that the mentioned compounds **1**-**6** followed the Lipinski rule with higher GI absorption and bioavailability score. So, they should be considered standard drugs. But ligands **7**-**9** didn't follow the rule due to their higher molecular weights. So, the molecular weight has been neglected, and we should continue further studies.

Table 1. Data on Lipinski rule, pharmacokinetics, and drug-likeness.

Ligand No.	NBR	HBA	HBD	TPSA, Å²	Consensus Log Po/w	Log Kp (skin permeation), cm/s	Lipinski rule Result	violation	M.W.	Bioavailability Score	G.I. absorption
1	01	05	03	79.15	-0.95	-8.49	Yes	00	178.18	0.55	High
2	01	05	01	57.15	0.53	-7.62	Yes	00	218.25	0.55	High
3	04	06	01	66.38	1.70	-6.91	Yes	00	304.38	0.55	High
4	04	06	03	88.38	0.21	-7.78	Yes	00	264.32	0.55	High
5	08	08	03	106.84	0.88	-7.78	Yes	00	352.42	0.55	High
6	08	10	05	197.90	0.05	-8.14	Yes	00	424.53	0.55	Low
7	20	08	03	106.84	5.16	-4.46	Yes	01	520.74	0.55	High
8	18	08	03	106.84	3.93	-4.34	Yes	01	524.77	0.55	Low
9	18	08	03	106.84	3.93	-4.34	Yes	01	524.77	0.55	Low
Fluconazole	05	07	01	81.65	0.88	-7.92	Yes	00	306.27	0.55	High

Abbreviation: TPSA: Topological polar surface area, Consensus Log: Logarithm of partition coefficient between *n*-octanol and water, NRB: Number of rotatable bonds, HBA: Hydrogen bond acceptor, HBD: Hydrogen bond donor, M.W: Molecular weight, G.I. Absorption: Gastrointestinal absorption

2.4 PASS assessment

A PASS prediction has been determined to identify the probability of active or inactive molecules [29]. The antiviral, antibacterial, antifungal, and antineoplastic profiles of all compounds were predicted using the PASS application (**1−9**). Pa and Pi, or PASS outcomes, are represented in Table 2. According to the prediction result in Table 3, it has been reported that the compounds **1−9** represented 0.440 < Pa <

0.580 for antibacterial, 0.367 < Pa < 0.730 for antifungal, 0.176 < Pa < 0.295 for antiviral, and 0.677< Pa < 0.920 for antineoplastic effects. The PASS prediction features have suggested that the reported compounds may be highly active against antineoplastics and fungal infections. So, based on this value, the black and white fungus has been selected for further analysis.

Table 2. Data for PASS prediction.

Ligand No.	Antiviral		Antibacterial		Antifungal		Antineoplastic	
	Pa	Pi	Pa	Pi	Pa	Pi	Pa	Pi
1	0.269	0.049	0.574	0.010	0.650	0.013	0.873	0.005
2	0.292	0.040	0.512	0.015	0.729	0.008	0.914	0.005
3	0.295	0.038	0.444	0.022	0.671	0.012	0.865	0.006
4	0.293	0.039	0.543	0.013	0.616	0.017	0.886	0.005
5	0.246	0.062	0.565	0.011	0.594	0.019	0.885	0.005
6	0.251	0.059	0.515	0.015	0.517	0.028	0.712	0.024
7	0.176	0.126	0.480	0.018	0.546	0.024	0.816	0.010
8	0.218	0.082	0.549	0.012	0.418	0.046	0.677	0.030
9	0.176	0.126	0.574	0.010	0.367	0.058	0.684	0.029
Fluconazole (CID 3365)	N/A	N/A	N/A	N/A	0.726	0.008	N/A	N/A

2.5 Molecular orbitals and chemical reactivity descriptors

Organic compounds and physiologically active molecules are distinguished by their chemical descriptors, which typically have profound significance [30]. The chemical descriptors of the mentioned molecules have been represented by εLUMO, εHOMO, and energy gap ($\Delta\varepsilon$), ionization potential (I), electron affinity (A), chemical potential (μ), electronegativity (χ), hardness (η), electrophilicity (ω), and softness (S) in Table 3 [31, 32]. The DFT application was used to calculate the relevant data for chemical descriptors. Molecular reactivity is higher when the energy gap between two molecules narrows [33].

Among these mentioned compounds,

rhamnopyranosides **6−9** have a smaller energy gap, whereas compounds **1−5** possess a greater energy gap. This value indicates that compounds **6−9** are much more reactive than those **1−5**. The highest electrophilicity index ω values for **6** (-6.2236 eV) and **9** (-5.8871 eV) indicated they were stronger electrophiles than mentioned compounds. Besides, from Table 3, it can be observed that a smaller value of softness is present in compound **2** (-0.1604 eV). When the functional groups have been added, their softness is increased (~-0.3205 eV) and similarly, the hardness value is reduced. According to the maximal hardness theory, the predicted hardness of the molecules should be more reactive, have strong bioactivity, and be more satisfactory for exploitation as medicines against black and white fungus [34, 35].

Table 3. Data on chemical descriptors.

S/N	A=-LUMO	I=- HOMO	Energy =I-A	Chemical potential $(\mu) = \frac{-I + A}{2}$	Electronegativity $(\chi) = \frac{I + A}{2}$	Hardness $(\eta) = \frac{I - A}{2}$	Softness $(S) = \frac{1}{\eta}$	Electrophilicity $(\omega) = \frac{\mu^2}{2}$
1	1.636	-10.654	12.290	4.5090	-4.509	-6.145	-0.1627	-1.6543
2	1.927	-10.538	12.465	4.3055	-4.3055	-6.2325	-0.1604	-1.4872
3	-1.211	-10.417	9.206	5.814	-5.814	-4.603	-0.2172	-3.6718
4	-1.459	-10.693	9.234	6.076	-6.076	-4.617	-0.2166	-3.9980
5	-1.958	-10.569	8.911	6.2635	-6.2635	-4.3055	-0.2323	-4.5560
6	-3.091	-10.374	7.283	6.7325	-6.7325	-3.6415	-0.2746	-6.2236
7	-1.862	-8.680	6.818	5.271	-5.271	-3.409	-0.2933	-4.0450
8	-2.743	-9.338	6.595	6.0405	-6.0405	-3.2975	-0.3033	-5.5326
9	-2.941	-9.181	6.240	6.061	-6.061	-3.120	-0.3205	-5.8871

2.6 Frontier Molecular Orbitals (HOMO and LUMO)

After optimization of the compounds using Density Functional Theory (DFT, B3LYP functional, and 6-31G++ basis sets), each of the molecules was opened in GaussView (a powerful tool for molecular visualization and analysis),

followed by navigation of its "Orbitals" section, selection of the HOMO and LUMO orbitals, visualization of their shapes, electron densities, and energy levels (http://users.df.uba.ar/rboc/em3/GAUSSIAN_TRAIN.pdf) [24, 35]. The saved orbitals were further modified in Material Studio 08 and presented here. Similar methods were used for

Molecular Electrostatic Potential (MEP) Maps. HOMO often corresponds to a possible high concentration of electrons in a region of a molecular structure where an electrophile may quickly engage atoms. It can be noticed in the visual illustration (Figure 3) that the HOMO region stretches onto the hydroxyl group. Due to the presence of electronegative oxygen atoms, their orbitals are more likely to contain HOMO configurations. After investigating their optimized structures, this research clearly demonstrated that this understanding of HOMO emanates from the frontier molecular orbital. On the other hand, the term LUMO implies the absence of electrons in a circumstance where a nucleophilic molecule may be readily substituted. The graphical illustration is presented in Figure 3.
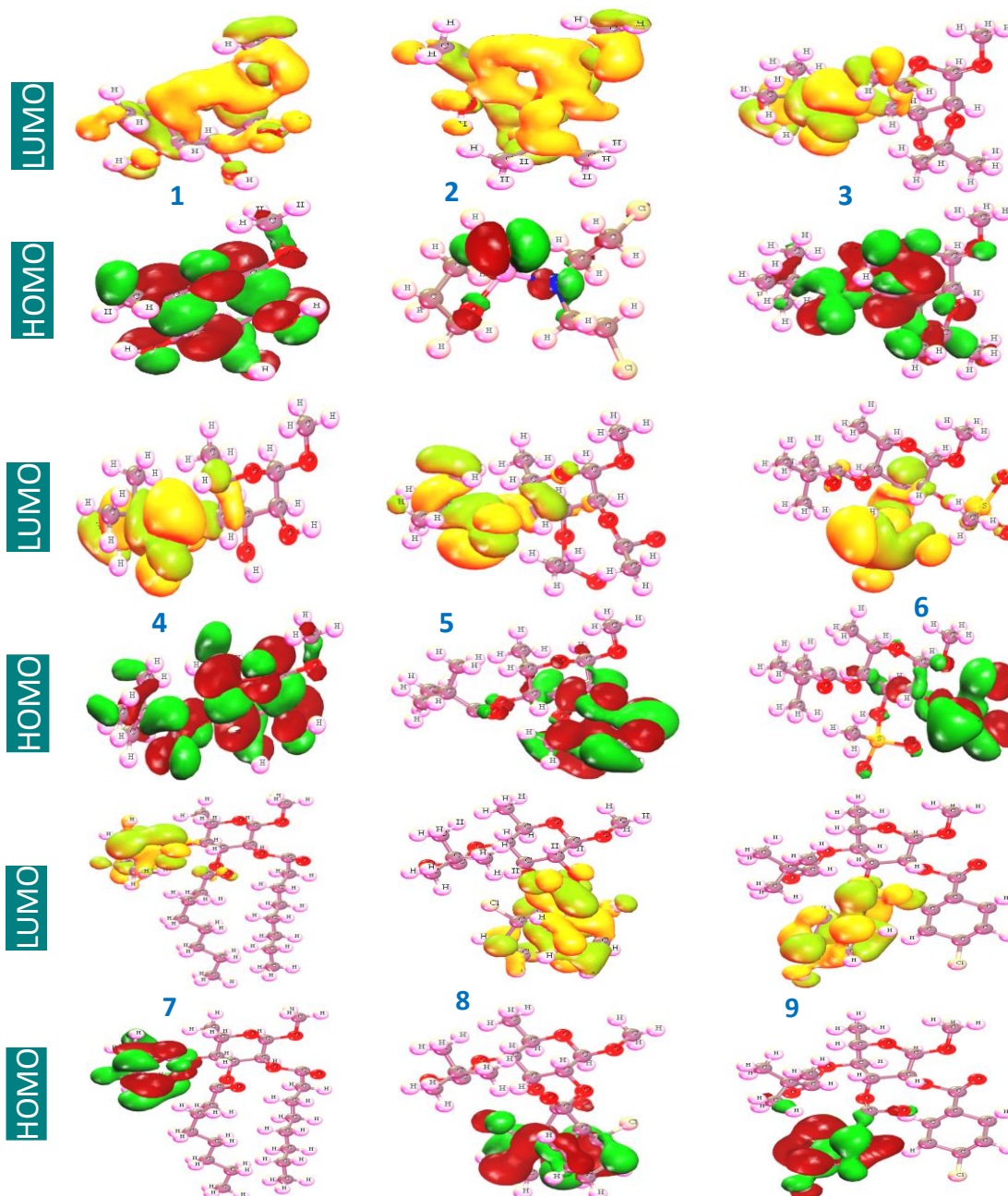

Fig. 3. Frontier Molecular Orbitals (HOMO and LUMO) of rhamnopyranoside **1** and its esters **2-9**.

2.7 Electrostatic potential map

The electrostatic potential of a compound is important to understanding and predicting the atom's reactivity. The interface of the molecular electrostatic potential (MEP) could represent the characteristics of the macromolecule's active terminal, including the comparative binding position and the types of the active site that indicate the electrophile attack [36]. The electrostatic potential structure of based-on-biology molecules is mapped by analyzing the substituent and electron-deficient zones of the chemical compound [37].

Predicting ligand engagement in biochemical reactions and the mechanics of their engagement may be understood by the molecular labels through this. Figure 4 shows an MEP surface visualization of black and white fungal protein ligand-binding areas with all docked compounds. The positive potential is assigned to the electrically impoverished parts (blue), while the negative potential is assigned to the dense electron sections (red), and the neutral potential is assigned to the white areas. This suggests that the molecules are polar and may actively engage in the binding region with reliable bonds.

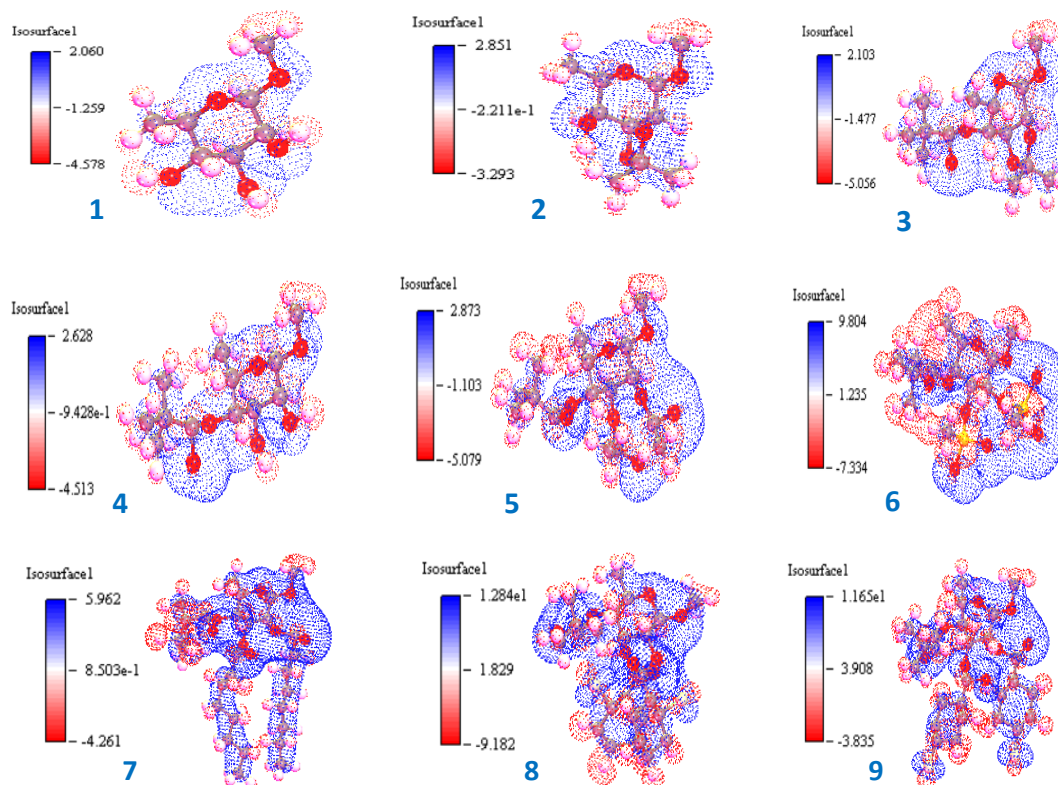Finally, inhibit the black and white fungal proliferation.

Fig. 4. Molecular electrostatic potential (MEP) mapping of **1**-**9**.

2.8 Molecular docking against black fungus

The molecular docking studies were conducted to assess the binding interactions and the ligands' binding orientations with regard to the protein binding site with four targeted proteins, including black and white fungus. Molecular docking has been performed to determine how much binding energy forms during the formation of a drug-protein complex, and affinities of -6.00 kcal/mol have been considered standard affinities [38]. According to the findings of the research (Table 4), **9** had the greatest interaction affinity or binding affinity among all the investigated compounds against black fungus proteins, which are -8.2 kcal/mol for *Mycolicibacterium smegmatis* (7D6X) and -8.7 kcal/mol for *Rhizomucor miehei* (4WTP). The ligands **3**, **5**, 7, and **8** have also opposed the standard affinities. At the same time, the standard fluconazole has shown -7.9 kcal/mol and -6.9 kcal/mol, which is lower than our finding.

Table 4. Binding affinity with black fungus.

Drug Molecules No.	*Mycolicibacterium smegmatis* (7D6X)			*Rhizomucor miehei* (4WTP)		
	Binding Affinity (kcal/mol)	No of H Bond	No of Hydrophobic Bond	Binding Affinity (kcal/mol)	No of H Bond	No of Hydrophobic Bond
1	-5.8	03	02	-5.7	03	00
2	-5.6	03	02	-6.4	05	03
3	-6.0	01	05	-6.3	01	09
4	-5.6	05	03	-6.2	02	06
5	-6.1	02	04	-6.4	05	02
6	-5.8	01	03	-6.0	01	05
7	-6.3	05	08	-6.4	02	13
8	**-7.2**	03	06	**-8.3**	01	08
9	**-8.2**	04	04	**-8.7**	00	10
Fluconazole	-7.9	07	04	-6.9	04	03

2.9 Molecular docking against white fungus

Additionally, the above-mentioned compounds were docked with the white fungus in order to detect their inhibitory impact. The docking investigation demonstrates that all of the compounds engage with the white fungus with a distinct ligand binding. The docking outcome has been represented in Table 5. On the basis of the outcome of Table 6, it is clear that compounds **8** and **9** have the maximum affinity for white fungus of all the investigated compounds, which is -7.0 kcal/mol against *Candida auris* (6U8J) in ligand **8** and -7.8 kcal/mol against *Aspergillus luchuensis* (1BK1) in ligand **9**. Besides, in every case, all the compounds have provided a different number of hydrogen and hydrophobic bonds, which play a fundamental role in the docking score.

Table 5. Binding affinity with white fungus

Drug Molecules No.	Candida auris (6U8J)			Aspergillus luchuensis (1BK1)		
	Binding Affinity (kcal/mol)	No of H Bond	No of Hydrophobic Bond	Binding Affinity (kcal/mol)	No of H Bond	No of Hydrophobic Bond
1	-5.6	04	01	-5.4	03	03
2	-5.5	01	07	-6.0	04	02
3	-5.7	04	05	**-7.0**	01	06
4	-5.6	02	04	-6.6	05	06
5	-5.4	06	05	-6.5	02	04
6	-5.2	03	02	-6.0	04	02
7	-6.1	00	14	-6.6	01	07
8	**-7.0**	02	03	**-7.6**	03	08
9	**-6.6**	01	03	**-7.8**	05	06
Fluconazole	-6.7	03	03	-7.5	05	06

2.10 Protein-ligand interaction

Protein and ligand interactions have been identified and designed by Pymol and Discovery Studio 2020 after the docking procedure is done. It has been used to analyze the docking sites or binding sites of the agonist and determine whether or not they are appropriate for the receptor once the docking simulation of the molecule is complete [39]. The main objective of protein-ligand interaction is to identify how accurately it binds to receptors. In Figure 5, different binding sites have been seen for different compounds.
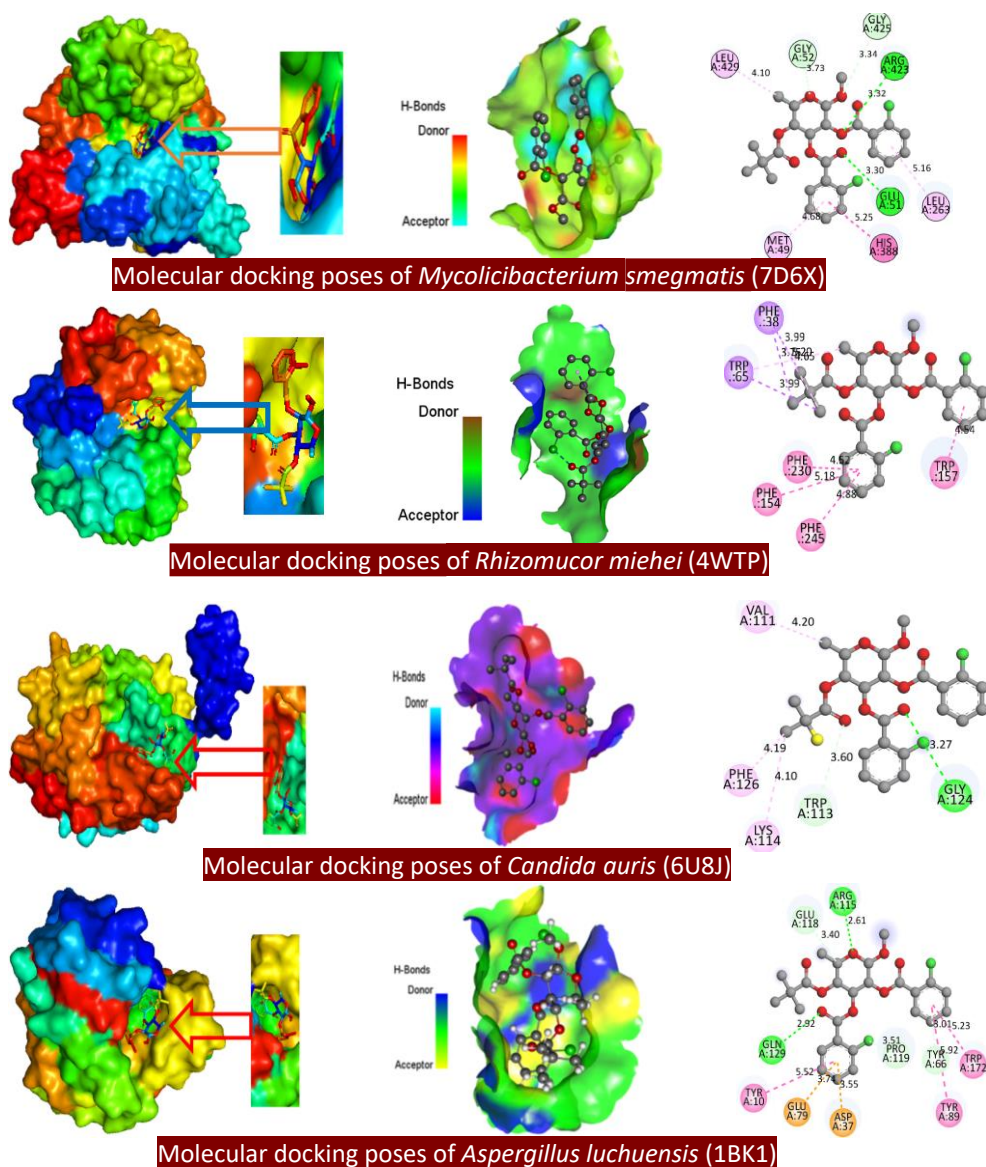

Molecular docking poses of *Mycolicibacterium smegmatis* (7D6X)

Molecular docking poses of *Rhizomucor miehei* (4WTP)

Molecular docking poses of *Candida auris* (6U8J)

Molecular docking poses of *Aspergillus luchuensis* (1BK1)

Fig. 5. Protein-ligand interaction pocket.

2.11 Molecular dynamics

Molecular dynamics simulation (MD simulation) is one of the well-established *in-silico* strategies for the evaluation of protein-ligand interaction, with a high resolution of the nanosecond or picosecond scale. This initiative has been conducted for testing the precision docking strategy in the possibility of the root-mean-square deviation (RMSD) and root-mean-square fluctuation (RMSF), which convey in priority their binding configuration ligand-protein complex after docking. A better fitting posture of the ligand in the drug pocket is defined as having a root mean square deviation (RMSD) of less than 2 Å for the docking complicated, and firmware can appropriately dock the ligand-protein complex

[40-42]. Docked complexes of compounds **8** and **9** with the maximum binding coefficients against the black fungus protein were identified. So, only the numbers **8**, **9**, and standard fluconazole were measured by applying molecular dynamics in this investigation.

In this study, the docked configuration of black and white fungus with synthesized organic molecules was employed at 100 ns for MD simulation and to evaluate the sustainability of the docked substances. The root-mean-square deviation (RMSD) values obtained from MD simulation disclose details on structural and conformational instability. The backbone RMSD data of fungal peptides and their complexes with therapeutics are depicted in Figure 6.
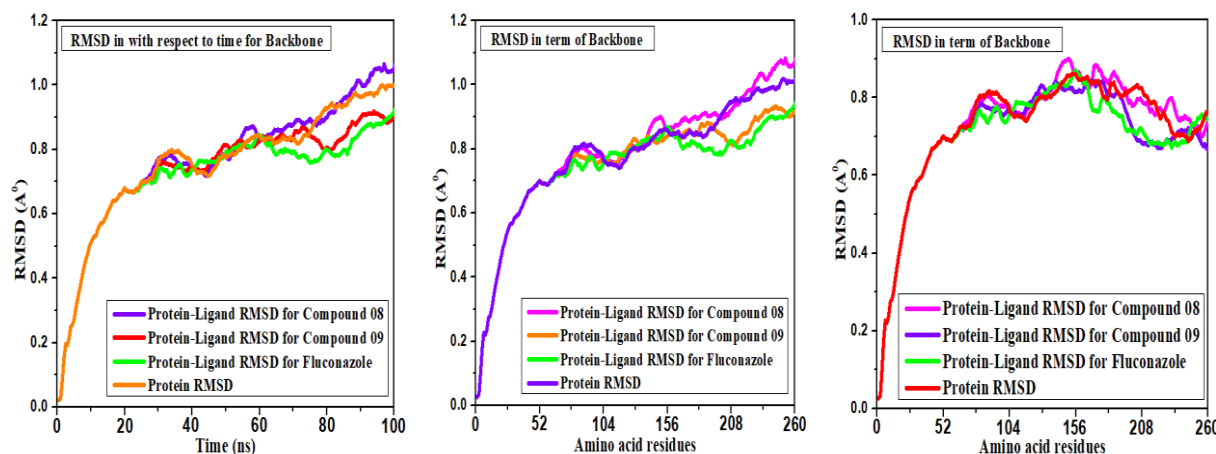

Fig. 6. MD simulation of compounds-4WTP complex.

It can be seen from the graphic of the MD simulation that the simulations exhibit less variation over the duration of the specified period at 100 ns. Firstly, the RMSD ratio was estimated to be 0.7 Å for all compounds, including fluconazole. But, when the time was increased, the RMSD values were also gradually increased, and each compound provided a different RMSD value at 100 ns. Compound **9** has provided a minimal RMSD value of 100 ns (0.8 Å). Similarly, amino acid residues *vs* RMSD have been looked up at equal for all compounds, and this has been slightly different at 260 for each compound, such that compound **8** has provided 10 Å, compound **9** has RMSD 0.9 Å, and the standard fluconazole has RMSD 0.9 Å.

2.12 ADMET studies

The pharmacokinetic characteristic of a bioactive compound is the most significant aspect to consider when selecting a new drug since it defines how the medication is absorbed, distributed, metabolized and finally excreted from the living system. The ADME (absorption, distribution, metabolism, and excretion) capabilities of a substance are the most important metrics that may be used to measure its pharmacokinetics. The potential drug candidates' pharmacokinetic parameters are given in Table 6.

Firstly, water solubility (log S) is a metric of the uniformity of a solution derived from a combination of solvent and solute that is evaluated. It is regarded as one of the most significant priorities in the estimation of drug concentrations in order to achieve the desired therapeutic efficacy [43]. Poor solubility in pharmaceuticals is a significant problem in the research and development of new therapeutics. Solubility serves as a stimulating factor in achieving high medication concentrations in the bloodstream, which is necessary for

therapeutic efficacy [44]. Our finding has been reported to be that the metric of solubility is -0.253 to -4.219. The standard values of log S for slightly solubilized and highly solubilized compounds vary from -4 to -6 and -2 to -4, respectively [45]. In accordance with their solubility parameters, these compounds have better solubility and should be administered orally.

On the other hand, BBB penetration and VDss are significant considerations for the diffusion of bioactive substances. Table 6 presents that, except for ligand molecule **3**, none of the ligand molecules can pass through the BBB, indicating that they could not distribute the BBB. The engagement of drug compounds with cytochromes P450 (CYP) is a significant feature since they contribute significantly to drug clearance via biotransformation metabolism. These compounds are not substrates or inhibited by these catalysts, as shown by CYP 450 such as CYP1A2 and CYP2C9, which is identical to the slow decomposition rate of these molecules and makes it adequately suitable for fighting the black and white fungus. All of these criteria suggest that these compounds are similar to potential drug-like compounds and should be exploited as effective drug candidates.

2.13. Aquatic and non-aquatic toxicity

Aquatic and non-aquatic toxicity have always been key requirements for new drug design since they may produce carcinogenicity or adverse effects in the environment through human excretion or during manufacturing [46]. It is estimated that all the compounds conducted in aquatic and non-aquatic toxicity experiments are eligible for medication development, with them being free from AMES (excluding **1** and **2**) and free from hepatotoxicity (Table 7). So, hepatic patients should use

these drugs. They are not skin sensitizers that are beneficial for the transdermal distribution of these drugs. Besides, the maximum tolerated human dose range among all compounds is 1.695 mg/kg/day. Lastly, the oral rat acute toxicity range is 1.521 mol/kg to 4.088 mol/kg, and the oral rat chronic toxicity range is 0.832 mg/kg/day to 3.551 mg/kg/day. All these findings recommend their utilization as an oral drug.

Table 6. ADME properties.

S/N	Absorption				Distribution		Metabolism		Excretion	
	Water solubility Log S	Caco-2 Permeability	P-glycoprotein substrate	P-I glycoprotein inhibitor	VDss (human)	BBB permeability	CYP450 1A2 Inhibitor	CYP450 2C9 Substrate	Total Clearance (ml/min/kg)	Renal OCT2 substrate
1	-0.253	0.553	No	No	-0.336	No	No	No	0.624	No
2	-1.196	1.171	No	No	-0.101	No	No	No	1.160	No
3	-2.312	-0.533	No	No	0.249	Yes	No	No	0.948	No
4	-1.410	0.275	No	No	-0.163	No	No	No	1.208	No
5	-2.377	0.124	Yes	No	0.643	No	No	No	1.346	No
6	-2.685	0.175	Yes	Yes	0.711	No	No	No	1.17	No
7	-3.097	1.042	Yes	Yes	0.870	No	No	No	1.689	No
8	-3.97	1.113	Yes	Yes	0.562	No	No	No	0.625	No
9	-4.219	1.091	Yes	Yes	0.442	No	No	No	0.374	No
Fluconazole	-2.666	1.104	No	No	-0.624	No	Yes	No	0.433	No

Table 7. Aquatic and non-aquatic toxicity.

S/N	AMES toxicity	Max. tolerated dose (human) mg/kg/day	Oral Rat Acute Toxicity (LD$_{50}$) (mol/kg)	Oral Rat Chronic Toxicity (mg/kg/day)	Hepato-toxicity	Skin Sensitization	T. Pyriformis toxicity (log ug/L)
1	Yes	1.695	1.521	2.133	No	No	-0.052
2	Yes	0.974	2.122	0.832	No	No	-0.41
3	No	0.414	2.61	1.459	No	No	0.329
4	No	0.488	1.837	2.178	No	No	0.267
5	No	0.583	2.04	2.799	No	No	0.285
6	No	0.476	2.778	3.551	No	No	0.285
7	No	0.006	4.088	2.624	No	No	0.285
8	No	-0.672	3.724	2.299	No	No	0.285
9	No	-0.89	3.723	2.471	No	No	0.285
Fluconazole	No	0.081	2.089	1.077	Yes	No	0.290

3. Material and Methods

3.1 Optimization and ligand preparation

Molecular optimization was carried out with the assistance of a method known as DFT functional, which made use of the vibrational frequency from the DMol3 code of Material Studio 08 to carry out the optimization [47]. The functional B3LYP was used for the renovation of operations in the DMol3 code in order to produce an extremely accurate outcome since the electronegative atom, oxygen, appeared to be present. Once the optimization procedure has been done, the frontier molecular orbitals (HOMO and LUMO), as well as the magnitude of HOMO and LUMO, were designed, among other things. In order to facilitate subsequent computational work, the optimized compounds were saved in PDB format for use in molecular docking, molecular dynamics, and ADMET.

3.2 PASS analysis

Web-based program PASS (**http://way2drug.com/PassOnline/predict.php**) has been applied to determine the antibacterial activity spectrum of the synthesized methyl α-L-rhamnopyranoside derivatives [48]. Over 4000 kinds of antimicrobial functions, including drug and non-drug activities, will be estimated by this system. This server allows the most suitable substances to be selected with optimum accuracy. In PASS experiments, Pa (the probability of an active molecule) and Pi (the probability of an inactive molecule) present the results. With possibility, the Pa and Pi values vary from 0.00 to 1.00 frequently [49].

3.3 *In silico* pharmacokinetics: ADMET and drug-like parameter prediction

Prior to conducting the molecular docking investigation, the recommended compounds were validated by the SwissADME (http://www.swissadme.ch) online database [50] for analyzing their Lipinski rule satisfaction since the Lipinski rule is one of the fundamental criteria for an oral drug [51].

Then, these have been considered for molecular docking after fulfilling all of Lipinski's prerequisites. In addition, the online database pkCSM accomplished the ADMET elements. According to this database, it is possible to accurately forecast the AMDET (absorption distribution metabolism excretion) characteristics [52].

3.4 Protein preparation

From the RCSB-Protein Data Bank, the crystal structure of the black and white fungus complex with *Mycolicibacterium smegmatis* (PDB ID 7D6X), *Rhizomucor miehei* (PDB ID 4WTP), *Candida auris* (PDB ID 6U8J), and *Aspergillus luchuensis* (PDB 1BK1) was collected for molecular docking procedures. Pymol application has been used to remove water molecules and heteroatoms from the crystal structure [53]. After that, the structural modification and energy minimization were realized using Swiss-PDB Viewer [54]. Finally, the clean geometry component was saved in PDB format, which is accessible on the Discovery Studio system, to conduct the amino acid residue assessment.

3.5 Molecular docking study and visualization

Molecular docking techniques are frequently utilized for estimating the binding interactions of a multitude of compounds, and they are becoming more prominent for finding active molecules [55, 56]. The auto-docking screening for the designated and synthesized derived molecules was evaluated for black and white fungus by PyRx [56, 57]. The grid box parameter was set to protein size and ligand. The grid box size has been listed in Table 8.

Table 8. Grid box parameters used for docking analysis in this study for fungi.

Protein Name with the PDB ID	Grid box size	
	Dimension (Å)	Center
7D6X	x = 72.8977702332 y = 74.5341963959 z = 55.288138504	x = 158.4178 y = 155.1521 z = 119.4373
1B1K	X = 41.6318564034 Y = 38.432412796 Z = 40.826666584	X = 27.2974 Y = 10.6735 Z = 35.7489
5HA9	X = 72.4786116028 Y = 48.9189193726 Z = 51.884504776	X = 17.4022 Y = 69.4248 Z = 90.3657
4WTP	X = 48.0575288868 Y = 41.7462174559 Z = 51.5023103333	X = 14.3218 Y = 27.7359 Z = 63.6785

In general, molecular modeling is used as a significant approach for the estimation of drug−macromolecule interactions, and it is extremely prevalent. This strategy contributes to improving the efficiency and effectiveness of the investigation while simultaneously reducing the cost of the laboratory.

3.6 Molecular dynamics (MD) simulations

MD simulations employing the NAMD program and an elevated laptop computer have been used to evaluate the stabilities of binding conformational interactions of these bioactive chemicals with four pathogenic fungal proteins. The MD simulation was used to support the docking results obtained for the optimum antifungal medications up to 5000 ns for holo-form (drug-protein) using the AMBER14 force field, which was applied to the docking observations [58]. With the addition of a liquid medium, the total system was adjusted with 0.9 percent NaCl at a temperature of 298 K. During the experiment, a square cell was cycled inside 20 Å on either side of the operation under periodic boundary conditions. VMD was used to determine RMSD and RMSF when the simulations were concluded

4. Conclusions

The new spread of the black fungus, in conjunction with the COVID-19 virus, has made the epidemiological predicament significantly worse. In this regard, this investigation has been performed by numerous rhamnopyranose-based derivatives with appropriate molecular orbitals, chemical reactivity descriptors, and molecular docking towards the black and white fungus-related pathogen. Based on molecular docking, MD simulations, ADMET, HOMO-LUMO, and PASS prediction results, some of these pivaloyl rhamnopyranosides have significant potential as effective medication candidates. Especially, compounds like methyl 2,3-di-*O*-(2-chlorobenzoyl)-4-*O*-pivaloyl-α-L-rhamnopyranoside (**8**) and methyl 2,3-di-*O*-(4-chlorobenzoyl)-4-*O*-pivaloyl-α-L-rhamnopyranoside (**9**) have been found to posess high potential for both black fungus (7D6X and 4WTP) and white fungus (6U8J and 1BK1). Encouragingly, it has been shown that the aforementioned derivatives are more effective as compared to presently available medications such as fluconazole, and hence further investigations are necessary.

Acknowledgments

Author Contributions

All authors contributed to the design and conception of the study. A computational study was performed by A. Kumer, S. Akash, and U. Chakma. MD simulation was performed by A. Chandro and U. Chakma. M. M. Matin performed validity and project management. The first draft of the manuscript was written by M. M. Matin, and all authors commented on previous versions and approved the final version of the manuscript.

References and Notes

[1]   Roden, M. M.; Zaoutis, T. E.; Buchanan, W. L.; Knudsen, T. A.; Sarkisova, T. A.; Schaufele, R. L.; et al. *Clin. Infect. Dis.* **2005**, *41*, 634. **[Crossref]**

[2]   Pal, R.; Singh, B.; Bhadada, S. K.; Banerjee, M.; Bhogal, R. S.; Hage, N.; et al. *Mycoses* **2021**, *64*, 1452. **[Crossref]**

[3]   Katti, V.; Ramamurthy, L. B.; Seetalakshmi, D. K.; Prakash, A. *Oman journal of ophthalmology*, **2023**, *16*, 268. **[Crossref]**

[4]   Daria, S.; Asaduzzaman, M.; Shahriar, M.; Islam, M. R. *Intl. J. Health Planning Management* **2021**, *36*, 1947. **[Crossref]**

[5]   Patidar, A.; Kayande, N.; Kushwah, P.; Birle, R.; Kushwah, N. *Int. J. Pharm. Life Sci.* **2021**, *12*, 9.

[6]   Walther, G.; Wagner, L.; Kurzai, O. *Mycopathologia* **2020**, *185*, 765. **[Crossref]**

[7]   Balwan1, W.K.; Saba, N.; Rasool, N. *Saudi J. Pathol. Microbiol.* **2021**, *6*, 187. **[Crossref]**

[8]   Lal, P. M.; Arif, A.; Mohan, A.; Rackimuthu, S.; Hasan, M.M.; Islam, Z., et al. *Clin. Epidemiol. Glob. Health* **2022**, *13*, 100960. **[Crossref]**

[9]   Moona, A. A.; Islam, M. R. *Public Health Pract* (Oxf). **2021**, *2*, 100153. **[Crossref]**

[10]   Nanditha, A.; Ma, R. C.; Ramachandran, A.; Snehalatha, C.; Chan, J. C.; Chia, K. S.; et al. *Diabetes Care* **2016**, *39*, 472. **[Crossref]**

[11]   Prakash, H.; Ghosh, A.K.; Rudramurthy, S.M.; Singh, P.; Xess, I.; Savio, J.; et al. *Med. Mycol*. **2019**, *57*, 395. **[Crossref]**

[12]   Jeong, W.; Keighley, C.; Wolfe, R.; Lee, W. L.; Slavin, M. A.; Kong, D. C. M.; Chen, S. C. *Clin. Microbiol. Infect.* **2019**, *25*, 26. **[Crossref]**

[13]   Gambhir, R. S.; Aggarwal, A.; Bhardwaj, A.; Kaur, A.; Sohi, R. K.; Mehta, S. *Roczniki Panstwowego Zakladu Higieny*, **2021**, *72*, 239. **[Crossref]**

[14]   Mehta, S.; Pandey, A. *Cureus* **2020**, *12*, e10726. **[Crossref]**

[15]   Quan, L.; Gu, J.; Lin, W.; Wei, Y.; Lin, Y.; Liu, L. *Chem. Commun.* **2019**, *55*, 8564. **[Crossref]**

[16]   Brynskikh, A. M.; Zhao, Y.; Mosley, R. L.; Li, S.; Boska, M. D.; Klyachko, N. L.; et al. *Nanomedicine* (Lond) **2010**, *5*, 379. **[Crossref]**

[17]   Leung, K.; Chakraborty, K.; Saminathan, A.; Krishnan, Y. *Nat. Nanotechnol*. **2019**, *14*, 176. **[Crossref]**

[18]   Leopardi, S.; Blake, D.; Puechmaille, S.J. *Curr. Biol*. **2015**, *25*, R217-R219. **[Crossref]**

[19]   Luna, J. D., Ponssa, X. S.; Rodríguez, S. D.; Luna, N. C.; Juárez, C. *Ophthalmic Surg. Lasers* **1996**, *27,* 706. **[Link]**

[20]   Ashu, E. E.; Korfanty, G. A.; Samarasinghe, H.; Pum, N.; You, M.; Yamamura, D.; Xu, J. *Infect. Drug Resist*. **2018**, *11*, 1549. **[Crossref]**

[21]   Berger, S.; El Chazli, Y.; Babu, A. F.; Coste, A. T. *Front. Microbiol*. **2017**, *8*, 1024. **[Crossref]**

[22]   Matin, M. M.; Matin, P.; Rahman, M. R.; Ben Hadda, T.; Almalki, F. A.; Mahmud, S.; et al. *Front. Mol. Biosci*. **2022**, *9*, 864286. **[Crossref]**

[23]   Forsberg, K.; Woodworth, K.; Walters, M.; Berkow, E. L.; Jackson, B.; Chiller, T.; Vallabhaneni, S. *Med. Mycol*. **2019**, *57*, 1. **[Crossref]**

[24]   Kumer, A.; Chakma, U.; Matin, M. M.; Akash, S.; Chando, A.; Howlader, D. *Org. Commun*. **2021**, *14*, 305. **[Crossref]**

[25]   Matin, P.; Rahman, M. R.; Huda, D.; Bakri, M. K. B.; Uddin, J.; Yurkin, Y.; et al. *BioResources* **2022**, *17*, 3025. **[Crossref]**

[26]   Muhammad, D.; Matin, M. M.; Miah, S. M. R.; Devi, P. *Orbital: Electron. J. Chem.* **2021**, *13*, 250. **[Crossref]**

[27]   Matin, M. M.; Islam, N.; Siddika, A.; Bhattacharjee, S. C. *J. Turk. Chem. Soc., Sect. A* **2021**, *8*, 363. **[Crossref]**

[28]   Benet, L. Z.; Hosey, C. M.; Ursu, O.; Oprea, T. I. *Adv. Drug. Deliv. Rev.* **2016**, *101*, 89. **[Crossref]**

[29]   Hanee, U.; Rahman, M. R.; Matin, M. M. *Phys. Chem. Res.* **2021**, *9*, 591. **[Crossref]**

[30]   Rahman, M. A; Matin, M. M.; Kumer, A.; Chakma, U.; Rahman, M. R. *Phys. Chem. Res.* **2022**, *10*, 195. **[Crossref]**

[31]   Parthasarathi, R.; Padmanabhan, J.; Subramanian, V.; Maiti, B.; Chattaraj, P. K. *J. Phys. Chem. A* **2003**, *107*, 10346. **[Crossref]**

[32]   Pearson, R. G. *Inorganic Chemistry*, **1988**, *27*, 734. **[Crossref]**

[33]   Sanaullah, A. F. M.; Devi, P.; Hossain, T.; Sultan, S. B.; Badhon, M. M. U.; Hossain, M. E.; et al. *Molecules* **2023**, *28*, 986. **[Crossref]**

[34]   Mohan, O.; Trinh, Q.T.; Banerjee, A.; Mushrif, S. H. *Mol. Simul.* **2019**, *45*, 1163. **[Crossref]**

[35]   Kumer, A.; Sarker, M.N.; Paul, S. *Intl. J. Chem. Technol*. **2019**, *3*, 26. **[Crossref]**

[36]   Politzer, P.; Laurence, P.R.; Jayasuriya, K. *Environ. Health Perspect*. **1985**, *61*, 191. **[Crossref]**

[37]   Gadre, S. R.; Suresh, C. H.; Mohan, N. *Molecules* **2021**, *26*, 3289. **[Crossref]**

[38]   Matin, P.; Hanee, U.; Alam, M. S.; Jeong, J. E.; Matin, M. M.; Rahman, M. R.; Mahmud, S.; Alshahrani, M. M.; Kim, B. *Molecules* **2022**, *27*, 4125. **[Crossref]**

[39]   Matin, M. M.; Bhattacharjee, S. C.; Chakraborty, P.; Alam, M. S. *Carbohydr. Res*. **2019**, *485*, 107812. **[Crossref]**

[40]   Talarico, C.; Gervasoni, S.; Manelfi, C.; Pedretti, A.; Vistoli, G.; Beccari, A. R. *Int. J. Mol. Sci*. **2020**, *21*, 2265. **[Crossref]**

[41]   Kumer, A.; Chakma, U.; Chandro, A.; Howlader, D.; Akash, S.; Kobir, M.E.; et al. *J. Chilean Chem. Soc*. **2022**, *67*, 5623. **[Crossref]**

[42]   Abbasi, H.; Fereidoonnezhad, M.; Mirveis, Z. *Bioint. Res. Appl. Chem*. **2022**, *12*, 588. **[Crossref]**

[43]   Savjani, K. T.; Gajja,r A. K.; Savjani, J. K. *ISRN Pharm.* **2012**, *2012*, 195727. **[Crossref]**

[44]   Bergström, C. A. S.; Larsson, P. *Int. J. Pharm*. **2018**, *540*, 185. **[Crossref]**

[45]   Rout, J.; Swain, B.C.; Tripathy, U. *J. Biomol. Struct. Dyn*. **2022**, *40*, 860. **[Crossref]**

[46]   Khaldan, A.; Bouamrane, S.; El-mernissi, R.; Maghat, H.; Sbai, A.; Bouachrine, M.; Lakhlifi, T. *Bioint. Res. Appl. Chem.* **2023**, *13*, 302. **[Crossref]**

[47]   Delley, B. *J. Phys. Condens. Matter* **2010**, *22*, 384208. **[Crossref]**

[48]   Matin, M. M.; Bhuiyan, M. M. H.; Kibria, S. M.; Hasan, M. S. *Pharm. Chem. J.* **2022**, *56*, 627. **[Crossref]**

[49] Stepanchikova, A. V.; Lagunin, A. A.; Filimonov, D. A.; Poroikov, V. V. *Curr. Med. Chem*. **2003**, *10*, 225. **[Crossref]**

[50] Kumer, A.; Sarker, N.; Paul, S.; Zannat, A. *Adv. J. Chem. Sect. A* **2019**, *2*, 190. **[Crossref]**

[51] Proudfoot, J. R. *Bioorg. Med. Chem. Lett*. **2005**, *15*, 1087. **[Crossref]**

[52] Pires, D. E.; Blundell, T. L.; Ascher, D. B. *J. Med. Chem*. **2015**, *58*, 4066. **[Crossref]**

[53] Seeliger, D.; de Groot, B. L. *J. Comput. Aided Mol. Des*. **2010**, *24*, 417. **[Crossref[**

[54] Rahman, M. A.; Chakma, U.; Kumer, A.; Rahman, M. R.; Matin, M. M. *Biointerface Res. Appl. Chem.* **2023**, *13*, 52. **[Crossref]**

[55] Dallakyan, S.; Olson, A. J. *Methods Mol. Biol*. **2015**, *1263*, 243. **[Crossref]**

[56] Kumer, A.; Chakma, U.; Matin, M. M. *Orbital: Electron. J. Chem.* **2022**, *14*, 15. **[Crossref]**

[57] Matin, P.; Nayeem, S. M. A.; Matin, M. M.; Rahman, M. R.; Das, S.; Chakraborty, D. *Egypt. J. Chem.* **2023**, *66*, 153. **[Crossref]**

[58] Skjevik, Å. A.; Madej, B. D.; Dickson, C. J.; Teigen, K.; Walker, R. C.; Gould, I. R. *Chem. Commun.* **2015**, *51*, 4402. **[Crossref]**

How to cite this article